# Re-entering Fast Ion Effects on NBI Heating Power in High-Beta Plasmas of the Large Helical Device

**Ryosuke SEKI[1], Kiyomasa WATANABE[1], Hisamichi FUNABA[1], Yasuhiro SUZUKI[1], Yutaka MATSUMOTO[2], Kiyotaka HAMAMATSU[3], Satoru SAKAKIBARA[1] and Satoshi OHDACHI[1]**

[1] National Institute for Fusion Science, Toki 509-5292, Japan
[2] Graduate School of Engineering, Hokkaido University, Sapporo 060-8628, Japan
[3] Japan Atomic Energy Agency, Naka, 311-0193, Japan

E-mail: seki.ryohsuke@lhd.nifs.ac.jp

**Abstract.** We calculate the heating power of the neutral beam injection (NBI) in the $\langle\beta\rangle = 4.8\%$ high-beta discharge achieved in the Large Helical Device (LHD). We investigate the difference of the heating efficiency and the heating power profile between with and without the re-entering fast ion effects. When the re-entering fast ion effects are taken into account, the heating efficiency in the co injection of the NBI (co-NBI case) is improved and it is about 1.8 times larger than that without the re-entering effects. In contrast, the heating efficiency with the re-entering effects in the counter injection of the NBI (ctr-NBI case) rarely differs from that without the re-entering ones. We also study the re-entering fast ion effects on the transport properties in the LHD high beta discharges. It is found that the tendency of the thermal conductivities on the beta value is not so much sensitive with and without the re-entering effects. In addition, we investigate the difference in the re-entering fast ion effects caused by the field strength and the magnetic configuration. In the co-NBI case, the re-entering fast ion effects on the heating efficiency increases with the decrease of the field strength. In the contrast, the re-entering fast ion effects in the ctr-NBI case rarely differs by changing the field strength.

*Keywords*: re-entering fast ion, high-beta plasma, heating power, Monte-Carlo calculation, large helical device

## 1. Introduction

The Large Helical Device (LHD) is a heliotron-type device with $\ell = 2/m = 10$, $A_{\rm p} = 5.8 - 8.3$, $B_{\rm ax}$ up to 3 T, and a helical divertor[1]. The typical plasma major radius $R_{\rm ax}$ and the averaged plasma minor radius $a_{\rm p}$ in vacuum are 3.6 m and 0.64 m, respectively. Here, $\ell$ and $m$ are the poloidal and the toroidal period number of the helical coils, $A_{\rm p}$ is a plasma aspect ratio, and $B_{\rm ax}$ is a magnetic field strength at $R_{\rm ax}$. Three tangential neural beam injection (NBI) systems and two perpendicular-NBI systems have been installed on the LHD. A volume-average beta, $\langle\beta\rangle$, reached more than 5% using these NBI in the low magnetic field ($B_{\rm ax}$= 0.425 T)[2, 3]. In a finite beta plasma of the LHD, the equilibrium magnetic field differs significantly from a vacuum magnetic field. The magnetic axis shifts torus outwardly because of the shafranov shift. The flux surfaces in the periphery of the plasma are destroyed by a finite beta effect[4]. In addition, the deviation between the orbits of the fast ions and their initial flux surfaces is large in the low field strength, in which high-beta discharges are commonly done in the LHD. Therefore, an accurate fast ion orbit tracing is required for the accurate evaluation of heating power profiles, which leads to the accurate estimation of a plasma confinement propriety.

The conventional evaluation of the heating power profile in the high-beta plasma has been done on the basis of the fast ion tracing in the magnetic coordinates such as the Boozer coordinates[5] because the equilibrium magnetic field in the high-beta plasma has been conventionally calculated in the magnetic coordinates. In the LHD, the evaluation of the heat conductivity has been done on the basis of the heating power with a simple NBI heating power evaluation code with the fast ion orbit tracing in the Boozer coordinates, FIT3D[6, 7]. In the FIT3D, the birth points of fast ions are calculated by using the Monte-Carlo method taking the divergence of the NBI into account. The fast ion orbits are traced from their birth points in the Boozer coordinates with the pitch angle scatter for 20 $\mu s$ (five times of the toroidal circulating time in a 180 keV fast ion produced by the tangential-NBI), and the birth points of the fast ions are assumed the averaged minor radial position over the orbits in order to take the finite orbit effects into account. The fast ions are assumed to slow down at their averaged "birth" points in the FIT3D. A velocity distribution and the heating power profile of the fast ions are evaluated by an analytical steady-state solution of the Fokker-Planck (FP) equation[8]. According to early works of the transport analyses in LHD high-beta plasmas using the FIT3D , it is shown that plasma confinement property decreases with the increase of $\langle\beta\rangle$[9].

However, there are pointed to be a lot of re-entering fast ions[10], in the LHD high-beta plasmas[11]. Here, re-entering fast ions are the fast ions which re-enter in the region of the closed flux surfaces after they have once passed out of the Last Closed Flux Surface (LCFS). Since these re-entering fast ions pass through out of the LCFS, they cannot be traced in codes using the magnetic coordinates such as Boozer coordinates, and they are regarded as the lost particles. In order to take the re-entering fast ion

effects into account, we have developed the Monte-Carlo code, MORH, on the basis of the orbit following in the real coordinates[12]. In the MORH, we use the equilibrium magnetic field calculated by the three-dimensional magnetohydrodynamic equilibrium code, HINT[13, 14], with the real coordinates. Using the MORH, we have already calculated the fast ion velocity distribution function for the tangential-NBI and the perpendicular-NBI in the finite beta plasma[12, 15]. There, the effects of re-entering fast ions on the distribution function are studied. It was found that there are a lot of the re-entering fast ions in both the tangential-NBI and the perpendicular-NBI in the finite beta plasma. Especially in the perpendicular-NBI and the co injection of the tangential-NBI, the re-entering fast ions have a large effect on the fast ion velocity distribution function.

In this paper, we calculate the heating power profile of the $\langle\beta\rangle = 4.8\%$ high-beta discharge achieved in the LHD experiments using the MORH code. Here, we use the temperature and the density measured in the LHD experiment, and the equilibrium magnetic field consistent with the measured temperature and density profiles is also used. The divergence of the NBI on the birth profile is taken into account. We investigate the difference of the heating efficiency and the heating power profile from the conventional heating power evaluation method. Especially, the re-entering fast ion effects on the heating power are investigated in detail. In addition, we also calculate the heating power by changing the field strength and the magnetic configuration, and the difference in the re-entering fast ion effects is studied. In Sec. 2, the re-entering fast ion effect and the heating power by the NBI in a high-beta discharge are shown. The dependence of the re-entering fast ion effects on the field strength and the magnetic configuration is discussed in Sec. 3. The conclusion is provided in Sec. 4.

## 2. Re-entering fast ion effects on NBI heating power profile in high-beta discharge.

### *2.1. Calculation condition.*

In order to study the re-entering fast ion effects on the NBI heating power profile, we calculate it using the Monte-Carlo code (MORH). In the MORH, the fast ion orbits can be traced in the region outside the LCFS, where the closed flux surface does not exist, as well as in the region inside the LCFS using the equilibrium magnetic field calculated by the HINT. A Monte-Carlo collision operator including the pitch angle scatter and the slowing down effects is used[12]. As a result of many fast ion orbit tracings with Coulomb collision, the heating power profile as well as the steady-state fast ion velocity distribution including the re-entering fast ion effects can be evaluated. In addition, the loss of re-entering fast ions due to the charge exchange (CX) reaction which greatly affects the confinement of re-entering fast ions can be also estimated in the MORH[12].

We investigate the effect of the re-entering fast ions on a high-beta discharge ($\langle\beta\rangle = 4.8\%$, $\gamma = 1.2$, $B_{\rm ax} = 0.425$ T) observed in the LHD experiment[2, 3]. Here,

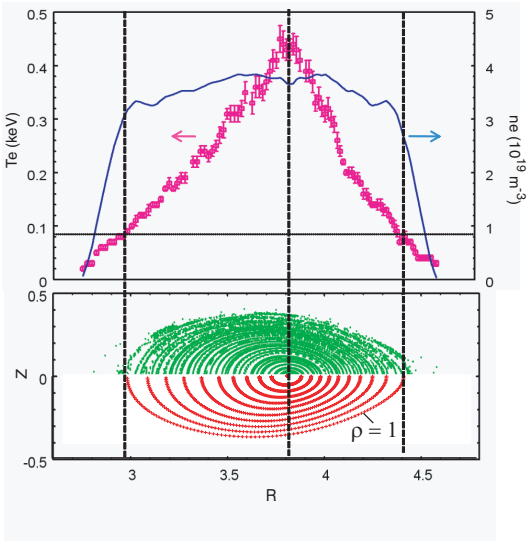


**Figure 1.** Electron temperature and electron density profiles (upper figure) and equilibrium magnetic field (lower figure) in the typical high beta discharge. In the lower figure, the Poincarè plot of magnetic field lines on the horizontally elongated poloidal plane is shown by green dots and the constant pressure surfaces are shown by red, where the outermost surface corresponds to LCFS (last closed magnetic surface, $\rho = 1$).

$\gamma$ is the coil pitch ($\gamma = ma_c/\ell R_c$, $R_c$ and $a_c$ are major and minor radii, respectively, of the helical coil). The electron temperature and the density profiles in the high beta discharge are shown in the upper figure of Fig. 1, and a Poincarè plot (upper side of lower figure) of magnetic field lines and constant pressure surfaces (lower side of lower figure) on the horizontally elongated poloidal plane are also shown in Fig. 1. The equilibrium magnetic field is calculated by HINT, and its field strength on the magnetic axis is 0.425 T. In the lower side in the lower figure of Fig. 1, the outermost constant pressure surface corresponds to the LCFS (normalized minor radius $\rho = 1$). Using the temperature and the density profiles measured in LHD experiments, the birth profile of the fast ions with the consideration for the NBI divergence are calculated by HFREYA[6] (Fig. 2). In the high-beta discharge, the fast ion produced by the NBI is a proton and its initial energy is about 180 keV. Using these conditions, the heating power profile is calculated by the MORH. In this study, the background plasma is assumed to consist of only one spice of ion, protons, and electrons. The ion temperature and the density are assumed to be equal to the electron temperature and the density, respectively. In the case that $T_\mathrm{e} = T_\mathrm{i} = 0.4$ keV and $n_\mathrm{e} = n_\mathrm{i} = 4 \times 10^{19}$ m$^{-3}$, it should be noted that energy relaxation times $\tau_{\mathrm{rel\_e}} = 3.7$ ms (for an electron), $\tau_{\mathrm{rel\_i}} = 530$ ms (for an ion), and pitch angle scatter times $\tau_{\mathrm{pi\_e}} = 1,491$ ms (for an electron), $\tau_{\mathrm{pi\_i}} = 530$ ms (for an ion). A toroidally circulating time of a typical passing fast ion produced by the tangential-NBI is about 5 $\mu s$. Because the energy relaxation time for the electron is much shorter than the pitch angle scatter times, most of the fast ions produced by the tangential-NBI stay

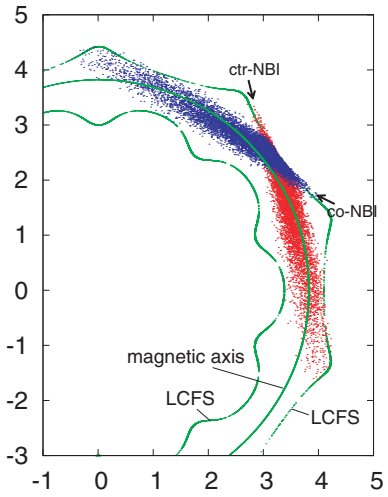


**Figure 2.** Projection of birth points of the NBI on the equatorial plan. Blue points show the birth points in the co-NBI case and red points show the birth points in the ctr-NBI case.

as the passing state during the slowing down. In this study, the uniform density of a hydrogen atom ($n_{\mathrm{H}}$) is assumed only outside the LCFS in order to investigate a effect of the CX loss on the re-entering fast ions.

### *2.2. Effect of re-entering fast ions on total heating power.*

In the high beta discharges, three tangential-NBIs are injected. Two tangential-NBIs are injected to the direction of field lines (co-NBI), another is injected counter to the direction of the field lines (ctr-NBI). Table 1 shows the effective heating powers ($Q_{\mathrm{abs\_eff}}$) calculated by the MORH in addition to the total port through powers ($Q_{\mathrm{port}}$), the total absorbed powers by plasmas ($Q_{\mathrm{abs}}$) by the experiment. Here, the total absorbed power ($Q_{\mathrm{abs}}$) is measured by a calorimeter. The effective heating power means a transported power from the fast ions to the background plasma. The effective heating power by the FIT3D is also shown as a reference. Here, the $n_{\mathrm{H}} = \infty$ case denotes the analyses without taking the re-entering fast ion effects into account, which correspond to the conventional analysis model using the Boozer coordinates, because all re-entering fast ions are lost due to the CX loss when $n_{\mathrm{H}} = \infty$. The effective heating power by the MORH in $n_{\mathrm{H}} = \infty$ case is less than that by the FIT3D. This difference is explained as followings. As shown in Sec. 1, in the FIT3D, the fast ions are traced for a very short time (20 $\mu$s) in order to estimate the effect of the fast ion orbit on the heating power profile. Because the tracing time is much shorter than the energy relaxation time ($\tau_{\mathrm{rel_e}} = 3.7$ms), a fast ion energy rarely changes from its initial energy for this tracing time. Therefore, the initial fast ion loss of the MORH is almost the same as the fast ion loss estimated by the FIT3D. In the MORH results, the fast ions are additionally lost due to the pitch angle scatter during slowing down. Thus, the heating power by the MORH ($n_{\mathrm{H}} = \infty$) is small compared with that by the FIT3D. In the table 1, the

**Table 1.** total heating power by NBI.

| | Port through power [MW] | Absorption power ($Q_{\rm abs}$) [MW] | Heating power by FIT3D [MW] | Heating power by MORH ($n_{\rm H} = \infty$) [MW] | Heating power by MORH ($n_{\rm H} = 0$) [MW] |
|---|---|---|---|---|---|
| co-NBI (NBI1+NBI3) | 9.132 | 7.853 | 5.155 | 4.278 | 7.770 |
| ctr-NBI (NBI2) | 4.169 | 3.781 | 1.975 | 1.708 | 1.756 |
| all NBI (NBI1+NBI2+NBI3) | 13.301 | 11.634 | 7.130 | 5.986 | 9.526 |

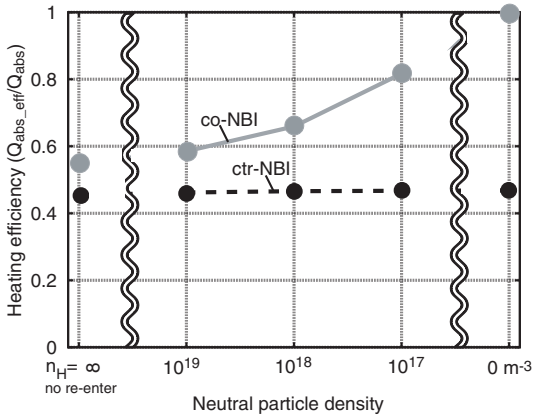


**Figure 3.** Heating efficiency as a function of the neutral hydrogen density outside the LCFS. The horizontal axis denotes the neutral hydrogen density ($n_{\rm H}$) outside the LCFS, and the vertical axis shows the heating efficiency ($Q_{\rm abs\_eff}/Q_{\rm abs}$). black and gray circles correspond to co-NBI and ctr-NBI cases, respectively.

effective heating power without taking the re-entering fast ions (MORH ($n_{\rm H} = \infty$)) into account is about 50% of the total absorbed power in both the co-NBI and the ctr-NBI cases. On the other hand, when the re-entering fast ion effects are included, the effective heating power of the co-NBI case becomes about 100% of the total absorbed power. The difference between the $n_{\rm H} = \infty$ and the $n_{\rm H} = 0$ cases in the co-NBI case is about 3.5 MW. In contrast, the effective heating power including the re-entering fast ion effects in the ctr-NBI case rarely differs from that without the re-entering effects. The reason of the difference between with and without the re-entering effects is discussed in Sec. 2.3.

Figure 3 shows the heating efficiency with the effects of the CX loss of re-entering fast ions. In this figure, the horizontal axis denotes the neutral hydrogen density ($n_{\rm H}$) in the outside of the LCFS, and the vertical axis shows the heating efficiency ($Q_{\rm abs\_eff}/Q_{\rm abs}$). In Fig. 3, the heating efficiency in the co-NBI case increases with the decrease of $n_{\rm H}$, while the heating efficiency in the ctr-NBI case is almost constant regardless of $n_{\rm H}$. In the LHD high-beta discharges, the typical value of the $n_{\rm H}$ measured by a fast ionization gauge is the order of $10^{18}$ m$^{-3}$. In the co-NBI case, the difference of the heating efficiency between with the $n_{\rm H} = 10^{18}$ m$^{-3}$ case and without the re-entering effects ($n_{\rm H} = \infty$) is about 10%, while the heating efficiency in the ctr-NBI case with $n_{\rm H} = 10^{18}$ m$^{-3}$ is almost equal to that without the re-entering effects ($n_{\rm H} = \infty$).

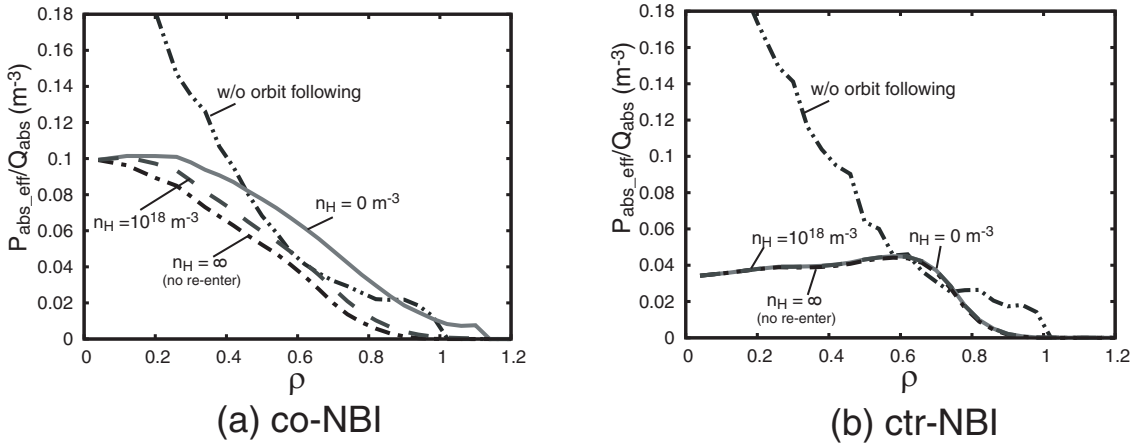


**Figure 4.** Heating efficiency profiles as a function of the minor radius, $\rho$, for various neutral hydrogen density cases. The horizontal axis shows the minor radius and the vertical axis shows the normalized heating power density. Figures (a) and (b) correspond to the co-NBI and ctr-NBI cases, respectively. Solid, dashed and dashed dotted lines correspond to the $n_{\rm H} = 0$, $10^{18}$ m$^{-3}$, $\infty$ cases, respectively. Dashed two dotted lines correspond to the w/wo orbit following case. $\rho = 1$ denotes the position of the LCFS, which is shown in Fig. 1.

### *2.3. Effect of re-entering fast ions on the heating power profile*

Figure 4 shows the heating power profiles by the NBI. In Fig. 4, the heating power profile evaluated without the particle tracing is also shown, which corresponds to the birth profile for the fast ions due to the NBI.

The birth profile of the fast ions peaks near the plasma center. On the other hand, in both the co-NBI and the ctr-NBI cases, the heating power by the MORH near the plasma center significantly decreases in comparison to the birth profile of the fast ions. In the co-NBI case (Fig. 4 (a)), the heating power profile becomes broad compared with the birth profile. In the ctr-NBI case (Fig. 4 (b)), the heating power profile in the core region is flat. In the co-NBI case, the heating powers in the $n_{\rm H} = 0$ are larger than that in $n_{\rm H} = \infty$ case over most of the plasma region. In the $n_{\rm H} = 10^{18}$ m$^{-3}$ case, the heating power in the co-NBI case is between in $n_{\rm H} = \infty$ and the $n_{\rm H} = 0$ cases and it is closer to that in $n_{\rm H} = \infty$ case. In the ctr-NBI case, the heating power profile in the $n_{\rm H} = 0$ case is same as that in the $n_{\rm H} = \infty$ case.

Next, we investigate the reason why there is the difference of the re-entering fast ion effects on the heating power profile between the co-NBI and the ctr-NBI cases. Here, the heating power profiles are plotted separately into two parts, the torus inside born ions and the torus outside born ones, because the characteristics of orbit between the torus inside born ions and the torus outside born ones are significantly different. In Fig. 5 (a), the birth profiles are plotted. The profile of the torus inside born ions is more peaked than that of the torus outside born ones. The number of the torus outside born ions are larger than the torus inside born ones. Here we should note that, in the co-NBI case, the torus inside born fast ions tend to move to the inner region of flux

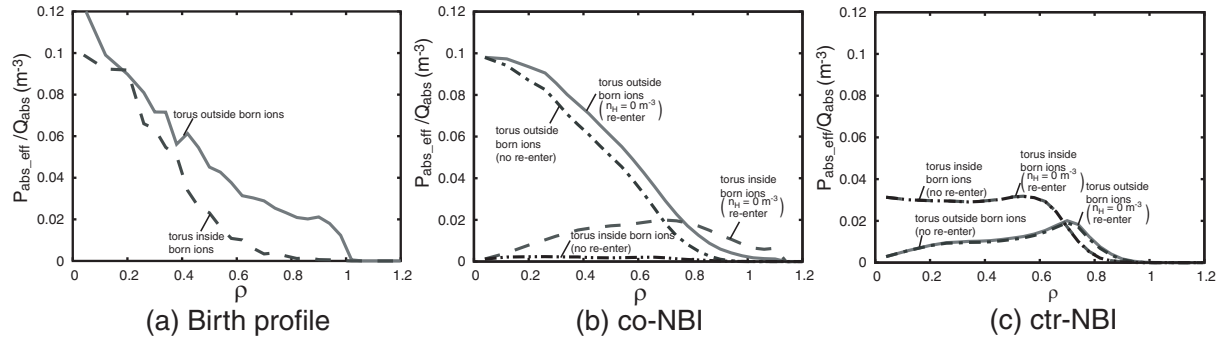


**Figure 5.** The heating efficiency profiles as a function of $\rho$ for (a) no orbit following case, (b) co-NBI case and (c) ctr-NBI case. Solid and dashed lines correspond to torus outside and torus inside born fast ions with $n_{\rm H} = 0$ in Fig. (b) and (c), respectively. Dashed dotted and dashed-two dotted lines correspond to torus outside and torus inside born fast ions with $n_{\rm H} = \infty$ in Fig. (b) and (c), respectively.

surfaces of their birth points as shown later in Fig. 11. In contrast, the torus outside born fast ions tend to move to the inner region of flux surfaces of their birth points. Then, some torus inside born ions pass through the LCFS. As shown in Fig. 5 (b), most of the torus inside born ions pass through the LCFS, which leads to the lost particles without the re-entering effects. This is because the distance between the torus outboard LCFS and the magnetic axis is smaller than that between torus inboard LCFS and the magnetic axis. On the contrary, as shown in Fig. 3, most of the ions which pass through the LCFS become the re-entering particles when the re-entering effects are taken into account. The reason is related with the properties of the radially vibrating motion of the fast ions from the co-NBI around the X-point as shown in Sec. 3. Here it should be noticed that the heating power profile as a function of $\rho$ has a hollow shape. On the other hand, for the torus outside born ions in the co-NBI case, the heating power profiles in the both cases with and without the re-entering effects are almost same, and on the absolute value the case with the re-entering effects is larger than that without the re-entering effects in the whole plasma region. This difference is because the torus outside born ions of which the birth points are far from the equatorial plane also move to the outer region of flux surfaces of their birth points without the collision. Here we should notice that, in the ctr-NBI case, the torus inside born fast ions tend to move to the inner region of flux surfaces of their birth points. In contrast, the torus inside born fast ions tend to move to the outer region of flux surfaces of their birth points. Then, some torus outside born ions pass through the LCFS. As shown in Fig. 5 (c), about half of the torus outside born ions pass through the LCFS, which leads to the lost particles without the re-entering effects. This is because the distance between the torus inboard LCFS and the magnetic axis is larger than that between torus outboard LCFS and the magnetic axis. In this case, most of the ions which pass through the LCFS do not become the re-entering particles even when the re-entering effects are taken into account. The reason is related with the properties of the radially vibrating motion of the fast ions from the ctr-NBI around the X-point as shown in Sec. 3. Most of the

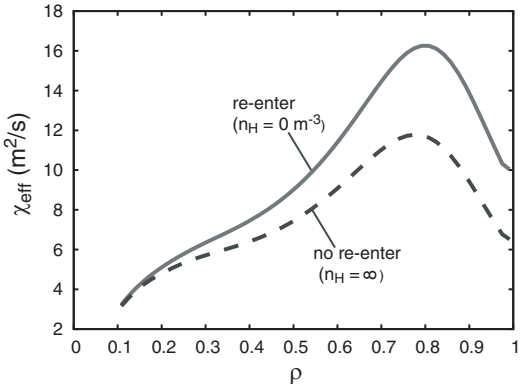


**Figure 6.** Thermal conductivity profile as a function of $\rho$. Solid and dashed lines correspond to the $n_{\rm H} = 0$ and $n_{\rm H} = \infty$ cases.

torus inside born ions is confined both cases with and without the re-entering effects. However the heating power profile as a function of $\rho$ has a flat shape. The reason is related with the properties of the energy transportation of the torus inside born ions during the slowing down time as shown in Appendix A.

### *2.4. Effect of re-entering fast ions on thermal conductivity*

By using the MORH code, we evaluate a thermal conductivity in the LHD high-beta plasmas. Here, the steady-state plasma in which heating powers balance the energy loss is assumed and the thermal conductivity is calculated by

$$\chi_j = -\frac{\int P_j V' \mathrm{d}\rho}{\langle |\nabla \rho^2| \rangle \, V' n_j \frac{\partial T_j}{\partial \rho}}, \tag{1}$$

where " j " denotes a particle species and $V' = \partial V / \partial \rho$. The convection term is ignored for simplicity. The thermal conductivity is calculated on the basis of the measured electron temperature and density shown in Fig. 1, assuming that $T_{\rm i} = T_{\rm e}$ and $n_{\rm i} = n_{\rm e}$. Then, the effective thermal conductivity is defined as[16]

$$\chi_{\rm eff} = \frac{\chi_e + \chi_i}{2}. \tag{2}$$

Figure 6 shows the effective thermal conductivity. The difference of the thermal conductivities between with the re-entering effect ($n_{\rm H} = 0$) and without the re-entering effects increases with the increase of the minor radius, and the local thermal conductivity near the LCFS ($\rho = 0.9$) with the re-entering effect is 40% larger than that without them. The above difference is explained as followings. As shown in Fig. 4 (a), the difference of the heating power between the re-entering effect ($n_{\rm H} = 0$) and without the re-entering effects in the co-NBI case is almost same in the whole plasma region. Since the volume element increases with the increase of the minor radius, the difference of the space integration of the heating power between the re-entering effect ($n_{\rm H} = 0$) and without the re-entering effects near LCFS is much larger than that near the core.

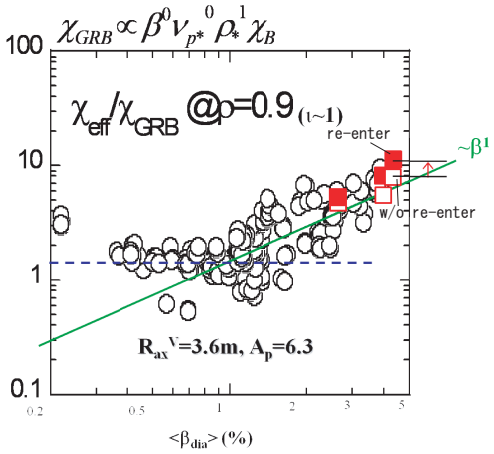


**Figure 7.** Effective thermal conductivities as a function as $\langle\beta_{\rm dia}\rangle$. The open circle denotes the effective thermal conductivities evaluated in the previous work, where the re-entering ion effects is not taken into account[9]. The open and the filled squares correspond to the results based on the MORH calculation without and with the re-entering effects, respectively. The solid and broken lines denotes $\beta^1$ dependence and $\beta^0$ dependence, respectively.

Next, we estimated how much the previously calculated confinement property changes due to the re-entering effect. Figure 7 shows the local thermal conductivity near the LCFS as a function of the beta value in the LHD experiments[9]. The open circles correspond to the thermal conductivities estimated by the conventional method of the NBI heating power, FIT3D[6]. The open squares denote the local thermal conductivity without the re-entering effects ($n_{\rm H} = \infty$), and the filled squares represent that with the re-entering effect, which corresponds to the result in the $n_{\rm H} = 0$ case.

In the typical LHD high-beta plasma maintained by the tangential-NBI, the central electron density ($n_{\rm e0}$) is 2-4$\times 10^{19}$ m$^{-3}$. In addition to the analysis for the $4 \times 10^{19}$ cm$^{-3}$ shown in Fig. 6, the thermal conductivities with the re-entering effect are plotted for $n_{\rm e0} = 3 \times 10^{19}$ and $2 \times 10^{19}$ m$^{-3}$ ($B_{\rm ax} = 0.9$ T). The thermal conductivity with the re-entering effect is slightly larger than the previously results of thermal conductivities. However, the difference between the re-entering effect ($n_{\rm H} = 0$) and without the re-entering effects is almost same with the scatter of the previously analyzed thermal conductivities. Because the typical value of the neutral hydrogen density in the outside of the LCFS in the high beta discharges is the order of $10^{18}$ m$^{-3}$, the reasonable thermal conductivity in the high beta discharge is between the closed squares and the open squares. Moreover, in the LHD, low-beta experiments are done at a higher magnetic field compared with that used in high-beta experiments. Then, the number of the re-entering fast ions decreases at the high field strength, and the effect of the re-entering fast ions in a low-beta discharge would be smaller than that in a high-beta discharge. Therefore, the dependence of the thermal conductivity taking the re-entering fast ion effect into account is a little different from that in the previous work, where the FIT3D

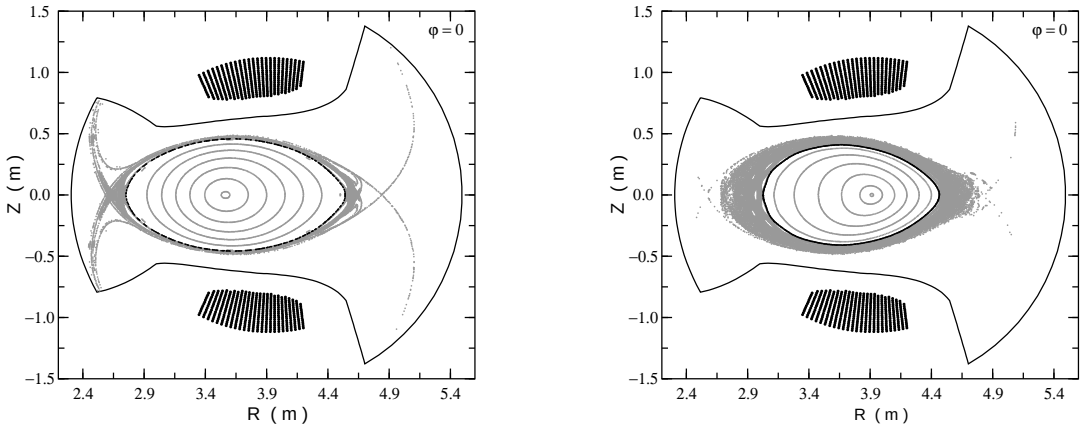


**Figure 8.** Poincarè plot of the magnetic field lines on the horizontally elongated poloidal plane in the LHD in the case of (a) vacuum magnetic field and (b) finite beta plasma. Black points denote the LCFS and Gray points the magnetic field lines. The vacuum vessel wall and helical coils of the LHD are also shown.

code is used and the re-entering fast ion effect is not taken into account.

## 3. Dependence of re-entering fast ion effects on the field strength and the magnetic configuration.

Here we discuss the re-entering fast ion effect on the heating efficiency due to the change of the deviation between the fast ion orbit and the flux surface through changing the field strength. And, we also study the re-entering effects due to the magnetic configuration, especially the major radius of the magnetic axis ($R_{\rm ax}$), on the heating efficiency through the comparison between the results for the finite beta configuration and the vacuum one. Figure 8 shows the Poincarè plots for the vacuum and the finite beta configurations. In this section, in order to clarify the differences of the re-entering fast ions effect due to the magnetic configuration, we consider the magnetic configuration with the smaller aspect ratio, in which the Shafranov shift is large. The magnetic configurations are exact same with as Fig. 1 in Ref. [11]. $R_{\rm ax} = 3.6$ m in vacuum. The magnetic axis in the finite beta plasma shifts torus outwardly because of the Shafranov shift and $R_{\rm ax} \simeq 3.9$ m. In the addition, the peripheral flux surfaces are destroyed by the finite beta effect as shown in Fig. 8 (b), which leads to that LCFS in the finite beta plasma is small compared with that in vacuum.

In this section, we assume that each beam line of the NBIs is a line (so-called pencile beam model) corresponding to the center of the NBI lines for simplicity. Here, birth points are set on the equatorial plane. Figures 9 (a) and 10 (a) show the birth points on the equatorial plane for the vacuum and the finite beta cases, respectively, which corresponds to the initial points for the orbit following of the fast ions. The birth points distributed in the radial locations in every $\Delta\rho = 0.1$ as shown in Figs. 9 and 10.

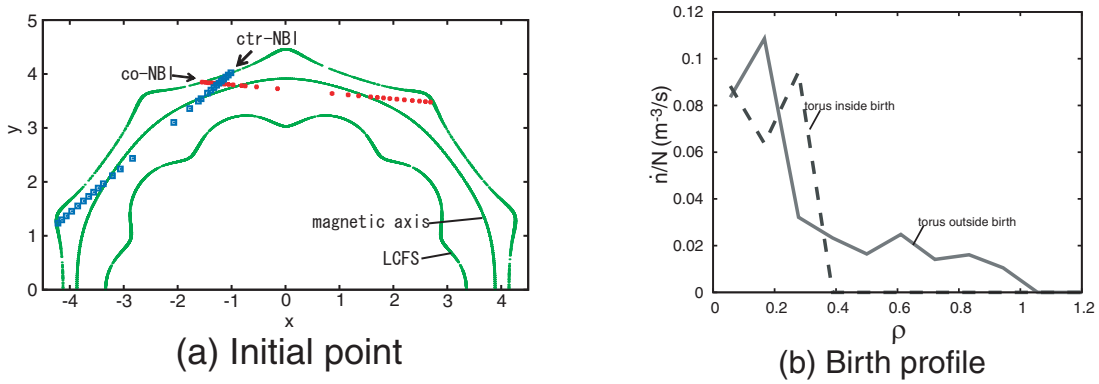


**Figure 9.** (a) Projection of birth points of the NBI on the equatorial plane in the vacuum field. Blue points shows the birth points in the co-NBI case and red points show the birth points in the ctr-NBI case. (b) The birth profile as a function of $\rho$.

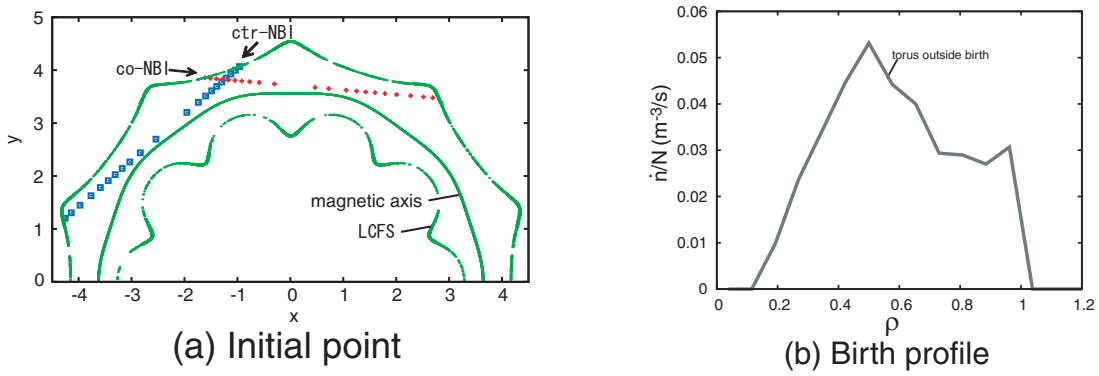


**Figure 10.** (a) Projection of birth points of the NBI on the equatorial plane in the finite beta configurations ($\langle\beta\rangle \sim 2.7\%$). Blue points shows the birth points in the co-NBI case and red points show the birth points in the ctr-NBI case. (b) The birth profile as a function of $\rho$.

Figures 9 (b) and 10 (b) show the birth profiles per unit volume as a function of $\rho$, for the vacuum and the finite beta cases, respectively. The birth profiles are given so that they are consistent with the birth profile with the divergence of the actual LHD NBI beam lines. The initial energy of the fast ion is assumed to be 180 keV, which corresponds to a typical value of the operational beam energy. The direction of the initial velocity of the fast ion is assumed same with the beam line. Here, the electron and the ion densities are assumed to be uniform, $n_e = n_i = 3 \times 10^{19}$ m$^{-3}$, and $T_e = T_i = 0.4 * (1 - \rho^2)$ keV.

Here we briefly review the properties of the fast ion guiding center orbits produced by tangential-NBI. Figure 11 shows the typical orbits for the co-NBI and the ctr-NBI cases with the various magnetic field strength and the magnetic configurations. In Fig. 11, the original point denotes the magnetic axis, and the horizontal axis corresponds to the normalized minor radius, $\rho$, where the minus and the plus regions correspond to the torus inboard side and the outboard side, respectively. The vertical axis is also represented by the normalized minor radius. In the case of the tangentially NBI, most fast ions become passing particles[11]. In the co-NBI cases (Figs 11 (a), (c)), the center

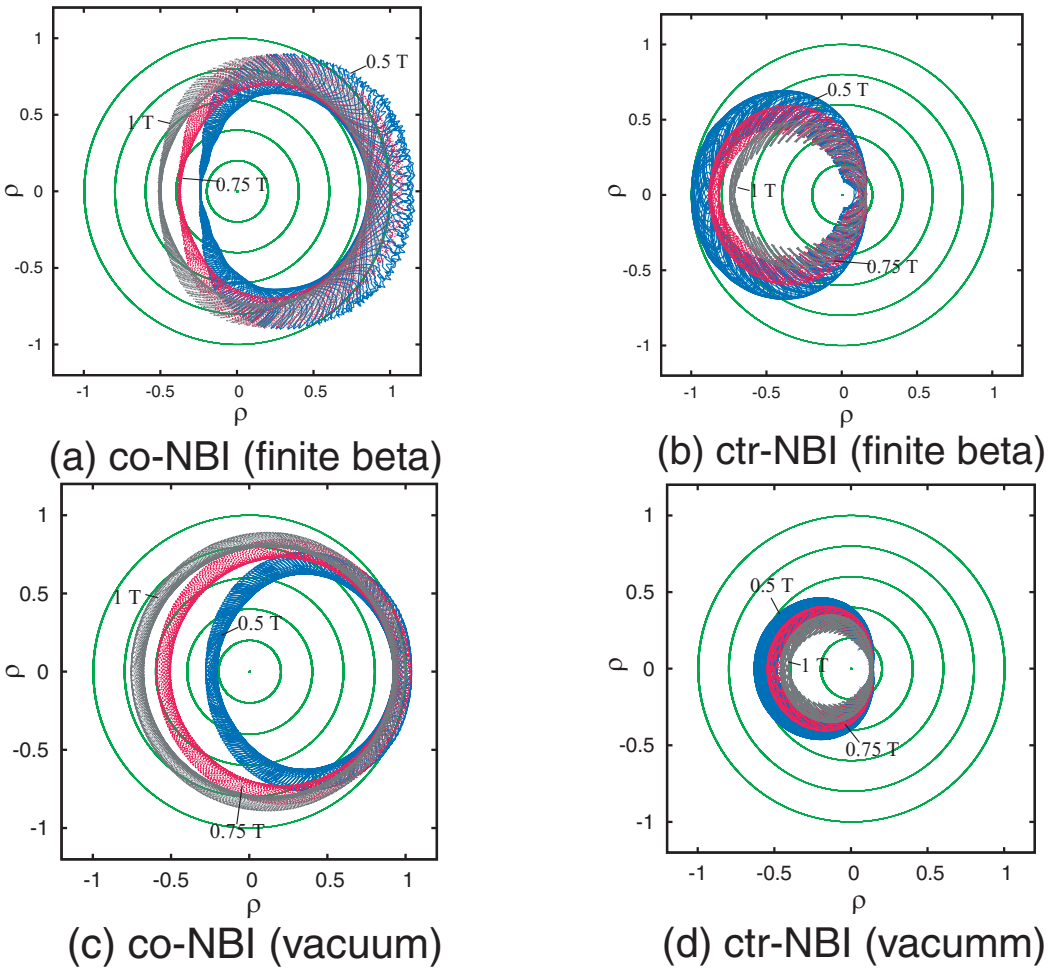


**Figure 11.** Typical orbit of the fast ion produced by tangential-NBI for various magnetic field strength. The original point shows the magnetic axis. The Horizontal axis denotes the major radius expressed in $\rho$ and the vertical axis corresponds to the direction of the main axis of the torus. (a) and (b) are for the finite beta cases ($\langle\beta\rangle \sim 2.7\%$). (c) and (d) are for the vacuum cases. (a) and (b) are for the co-NBI cases, and (b) and (d) are for the ctr-NBI cases.

of the fast ion guiding center orbit shifts to the torus outboard compared with the magnetic axis. Thus, the fast ions born in the torus outboard side pass through inner region of flux surfaces of their birth points, while the fast ions born in the torus inboard side pass through outer region of flux surfaces of their birth points. In the ctr-NBI case (Figs 11 (b), (d)), the center of the fast ion guiding center orbit shifts to the torus inboard compared with the magnetic axis. Thus, the fast ions born in the torus outboard side and inboard side pass through outer and inner regions of flux surfaces of their birth points, respectively. In both the co-NBI and the ctr-NBI cases not depending on the magnetic configurations (the vacuum and the finite beta), the deviation of the fast ion orbit from the flux surfaces become large with the decrease of the field strength. For example, the fast ion passes through near both the LCFS and the magnetic axis in the $B_{\rm ax} = 0.5$ T in the co-NBI and the ctr-NBI cases in the finite beta magnetic configuration

as shown in Figs. 11 (a) and (b). That is, most of fast ions in the magnetic field strength less than 0.5 T pass through out of the LCFS. According to more detail analysis of the fast ion guiding center orbit following[11], the particles which reach the divertor traces beyond the X points reach the vacuum vessel and they cannot re-enter in the closed magnetic flux region again. In the other words, the fast ions which do not reach the divertor traces become re-entering fast ions. From Fig. 11, we should note that the guiding center of the fast ions, which is categorized so-called 'passing particles', moves vibrationally in the minor radial direction in addition to the mainly poloidal direction. The minor radially vibrational motion is mentioned in detail in Ref. [11]. The minor radial motion is made by the drift of $\nabla_\theta B$ which is caused by helical coils of LHD. In the co-NBI case, the direction of the $\nabla_\theta B$ drift changes from the outward-directed drift to the inward-directed one near the helical coils. On the contrary, near the X points, it changes from inward-directed drift to the outward-directed one. As the results, in the co-NBI case, the particles near the coils are in the radially outer location in the minor radial vibrational motion, and those near the X points are in the radially inner location. In contrast, in the ctr-NBI case, the direction of the $\nabla_\theta B$ drift changes from the inward-directed drift to the outward-directed one near the helical coils, which leads that the particles near coils are in the radially inner location in the minor radial motion, and those near the X points are in the radially outer location. The above characteristics of the fast ion orbits strongly relates with the lost particles behavior in the co-NBI and the ctr-NBI cases with and without the re-entering effects shown in Figs. 3 and 5.

Now, we discuss the re-entering fast ion effects of the field strength on the heating efficiency of the tangential-NBI in order to know the effect of the orbit size on the heating efficiency. Figure 12 (a) shows the heating efficiency in the finite beta configuration as a function of magnetic field strength for the co-NBI and the ctr-NBI cases. In the co-NBI case, the difference between with and without the re-entering effects is not apparent above $B_{\rm ax} = 0.75$ T. On the other hand, below $B_{\rm ax} = 0.75$ T, the difference between with and without the re-entering effects is apparent. The reason of the above mentioned difference is in principle same with Fig. 5 (b) as already mentioned. Here an additional explanation is shown as follow. In this co-NBI case, most of the fast ions born in the torus inside are produced in $\rho < 0.4$ in the finite beta configuration case. In the fairly high magnetic field strength case like $B_{\rm ax} > 0.75$ T, the fast ions do not move beyond the LCFS because the distance between the LCFS and the flux surfaces of their birth points is farther than the deviation of the fast ion orbit from the flux surface. On the contrary, in the low field strength like $B_{\rm ax} < 0.75$ T, some fast ions born in the torus inside pass through out of the LCFS since the deviation of the fast ion orbit from the flux surface is large enough. However, when the re-entering fast ions are taken into account, the fast ions do not move beyond the X points even in $B_{\rm ax} = 0.5$ T since the fast ions near the X-points are in the radially inner location in the radially vibrational motion. Then, the re-entering fast ions are rarely lost in the co-NBI case. In addition, the fast ions born in the torus outside contribute the plasma heating both cases with and without the re-entering effects since they pass through the radially inner flux surfaces

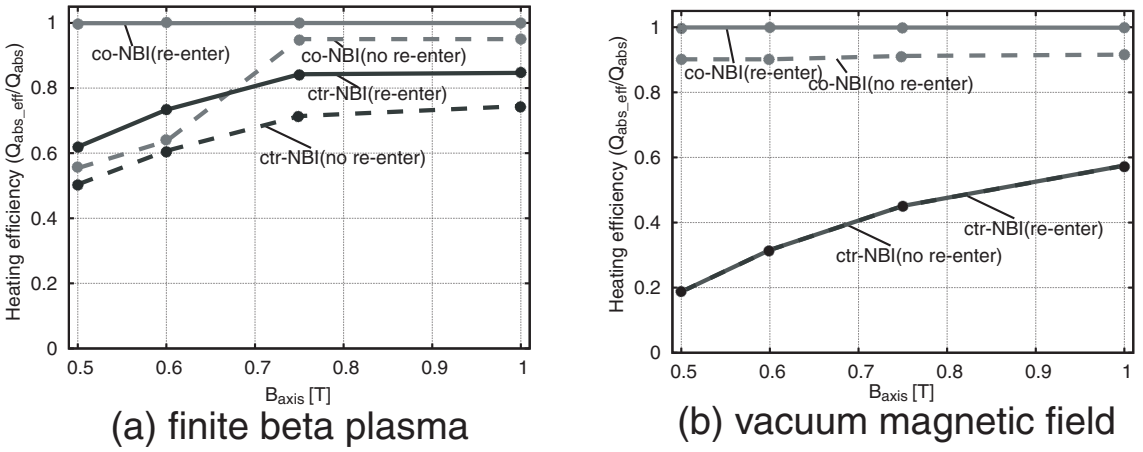


**Figure 12.** Heating efficiency as a function of the magnetic field strength for (a) the finite beta case ($\langle\beta\rangle \sim 2.7\%$) and for (b) the vacuum case. Solid and dashed lines denote with the re-entering effect ($n_{\rm H} = 0$) and without the re-entering effects ($n_{\rm H} = \infty$), respectively.

compared with their birth points, which leads that the re-entering effect is apparent below $B_{\rm ax} < 0.75$ T. In the ctr-NBI case, the heating efficiency decreases as the field strength decreases both cases with and without the re-entering effects. In this ctr-NBI case, as shown in Fig. 9 (b), the fast ions born in the torus outside are distributed in the whole plasma region. The fast ions born in the torus outside and in the minor-radially peripheral region pass through the LCFS even in the high $B_{\rm ax}$ case, and most of fast ions pass through the LCFS in $B_{\rm ax} = 0.5$ T as shown in Fig. 11 (b), which leads to the lost particles in the case without the re-entering effects. In the ctr-NBI case, since the fast ions near the X points are in the radially outer location, the fast ions easily move beyond the X points, which leads to the lost particles. Since the decrease of the field strength enhance the deviation between the orbit and the flux surface, the lost particles increase with the decrease of the field strength even with the re-entering effect.

Next, we discuss the re-entering fast ion effects of the magnetic configurations on the heating efficiency of the tangential-NBI through the comparison between the vacuum and the finite beta cases as shown in Fig. 12. Figure 12 (b) shows the heating efficiency in the vacuum configuration as a function of magnetic field strength for the co-NBI and the ctr-NBI cases. In the co-NBI case, the difference of the heating efficiency between with and without the re-entering effects in $B_{\rm ax} = 1$ T of the vacuum case rarely change from the finite beta plasma case. On the other hand, there is the significant difference of the re-entering fast ion effect between the finite beta and the vacuum cases in the $B_{\rm ax} = 0.5$ T. In the finite beta configuration, the difference between with and without the re-entering effects in $B_{\rm ax} = 0.5$ T is larger than that in $B_{\rm ax} = 1$ T as mentioned before. On the contrary, in the vacuum configuration, the difference in $B_{\rm ax} = 0.5$ T is almost same with that in $B_{\rm ax} = 1$ T. The above difference in the re-entering effects on the heating efficiency is caused by the location of the magnetic axis. In the finite beta configuration, the fast ions are born in the torus inside as well as the torus outside

because the magnetic axis shifts torus outwardly compared with the NBI lines. On the other hand, fast ions in the vacuum configuration are born only in the torus outside. In addition, the fast ions born in the torus outside pass through the radially inner of the birth points and they do not pass through out of the LCFS. Then, the number of re-entering fast ions in the vacuum case is smaller than that in the finite beta configuration in the co-NBI case. In the ctr-NBI case(compared with Figs. 12 (a) and (b)), regardless of the field strength, there is the difference of heating efficiency between with and without the re-entering effects in finite beta configuration, while the heating efficiency with the re-entering effects rarely differs from that without the re-entering effects in the vacuum case. This is because of the width of the stochastic magnetic field structure outside the LCFS. Since the fast ions which can move beyond the X point are lost, the"re-entering region" is defined as a region between the LCFS and the X points. Around the X point in the torus inside at the poloidal cross-section with the horizontally elongated flux surfaces, the distance between the LCFS and the X point is about 50 cm in the finite beta configuration, while the distance is about 20 cm in the vacuum configuration as shown in Fig. 8. Therefore, the fast ions in the finite beta configuration become more easily the re-entering fast ions than that in the vacuum configuration because the "re-entering region" in the finite beta configuration is larger than that in the vacuum configuration. The heating efficiency in the vacuum configuration itself is smaller than that in the finite beta configuration. For example, the heating efficiency in the finite beta configuration is about 0.5 even in the low magnetic field strength with $B_{\rm ax} = 0.5$ T, while that in the vacuum is about 0.2. This is because of the birth points. In the vacuum configuration, most fast ions are born only in the torus outside, where the fast ions easily move beyond the X points, which leads to the poor heating efficiency.

## 4. Conclusion

Using a Monte-Carlo code, MORH, on the basis of the orbit following in the real coordinates, we study the heating power profile of the tangential-NBI and the transport properties in the LHD high beta discharges, especially focusing on the re-entering fast ion effects. We also study the re-entering fast ion effects of the field strength and the magnetic configuration on the NBI heating power profile. The following results are obtained.

In the analysis on the LHD high beta discharges, the heating efficiency without the re-entering effects in both the co-NBI and the ctr-NBI cases is about 50% in the LHD high-beta plasma ($B_{\rm ax} = 0.425$ T). When the re-entering fast ions are taken into account, the heating efficiency in the co-NBI case becomes about 1.8 times larger than that without the re-entering effects. In contrast, the heating efficiency with the re-entering effects in the ctr-NBI case rarely differs from that without the re-entering effects. This difference of the re-entering effects between the co-NBI and the ctr-NBI cases is because the re-entering fast ions in the ctr-NBI case are more easily lost in comparison to the co-NBI case due to the drift of $\nabla_\theta B$ which is caused by helical coils

of LHD. As the results of the transport analysis, we confirm that the tendency of the thermal conductivities on the beta value is not so much sensitive with and without the re-entering effects.

Moreover, the re-entering fast ion effects on the heating efficiency by changing the magnetic field strength and the magnetic configurations are analyzed. In the co-NBI case with the re-entering effects, the heating efficiencies in both the finite beta and the vacuum configurations rarely differ by changing the field strength and the heating efficiencies are almost 100%. On the other hand, in the co-NBI case without the re-entering effects, the heating efficiency decreases with the decrease of the field strength in the finite beta configurations and does not change with the decrease of the field strength in the vacuum case. In the contrast, in the ctr-NBI case, the heating efficiency decreases with the decrease of the field strength in both cases with and without the re-entering effects. The re-entering effects on the heating efficiency is small in the vacuum case, and that in the finite beta case is relatively large. It is found that the difference of re-entering effects between the vacuum and the finite beta cases is caused by the width of the stochastic magnetic field structure outside the LCFS.

**Acknowledgments**

We thank Dr. M. Osakabe (National Institute for Fusion Science (NIFS)) for giving us information about the LHD NBI systems. We are grateful to Dr. M. Kobayashi (NIFS) for giving us information about the neutral density in the periphery region of the LHD. We are also grateful to the LHD experiment group and the LHD operation group for their support. This work is supported by the budget NIFS10ULPP022 and NIFS10KLPR003 of NIFS.

## Appendix A. Effects of the collison during slowing down on the heating power profile.

In this paper, we study the effects of the re-entering fast ions on the heating power profile of the NBI. Here, we discuss in detail the difference between of the heating power profile by a simple heating power evaluation code, FIT3D, which has been commonly used for transport studies in the LHD, and the MORH code except for the re-entering fast ion effect. In the FIT3D, the differences from the MORH are as followings in the addition to takeing the re-entering fast ion effects into account or not.

(i) The effect of fast ion orbit on the heating power profile is taken into account by tracing fast ions orbits from the birth points for the five toroidally circulating time. The averaged minor radial position is assumed the birth point of the fast ions taking finite orbit effect into account.

(ii) The fast ions are assumed to slow down at the "birth" points including the above finite orbit effect. The velocity distribution and the heating power profile are evaluated by an analytical steady-state solution of the Fokker-Planck (FP) equation.

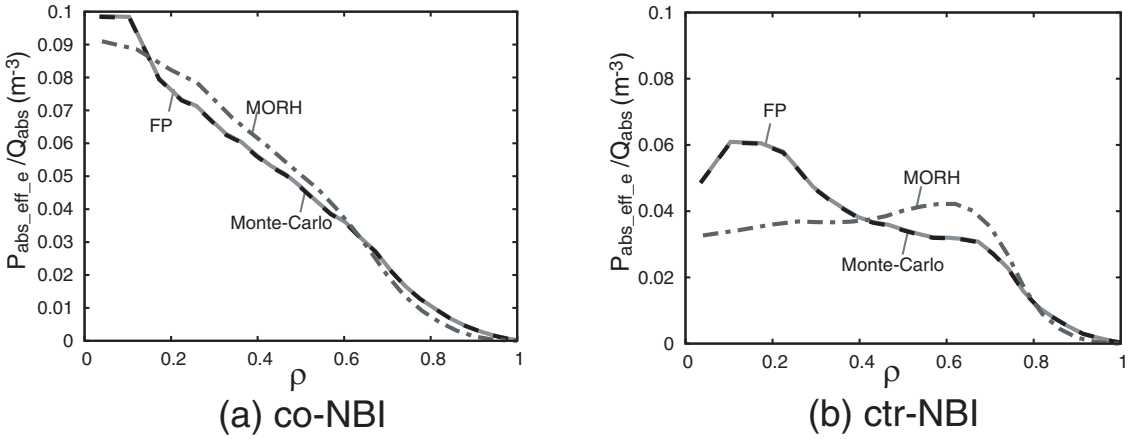


**Figure A1.** Electron heating power profiles as a function of $\rho$ for (a) the co-NBI case and (b) ctr-NBI case. Solid and dashed lines correspond to results calculated by the Monte-Carlo collision calculation and the steady state FP solution with slowing down at the birth point, respectively. The dotted dashed line corresponds to results calculated by the Monte-Carlo calculation with orbit following during slowing down, which is corresponding to the MORH's standard results.

In order to investigate the effects of the above two differences, the heating power are evaluated by using the Monte-Carlo collision operator[12] used in MORH (Monte-Carlo) and by the steady-state solution of the Fokker-Planck (FP). In the collision operator used in the MORH, the pitch angle scatter and the slowing down are considered, and the probabilistic energy transport from the back ground plasma to fast ions is also included. The magnetic field configuration and the back ground plasma parameter are the same as those shown in Fig. 1.

Figure A1 shows the heating power profile to the electrons as a function of $\rho$ in (a) the co-NBI and (b) the ctr-NBI cases. 'Monte-Carlo' and 'FP' correspond to results calculated by the Monte-Carlo collision calculation and the steady state FP solution with slowing down at the birth point, respectively. 'MORH' corresponds to results calculated by the Monte-Carlo collision calculation with orbit following during slowing down. Here 'FP' corresponds to the result by FIT3D. The heating power of 'FP' is almost same with that of 'Monte-Carlo'. In the co-NBI case, the heating power profiles as a function of $\rho$ are still peaked though they are broader than the birth profiles due the finite orbit effect. The heating power of 'MORH' in the center is a little smaller than the others, that in the core is a little larger and that near the LCFS is a little smaller. In this case, the density profile is flat in most of the plasma region and decreases only near the LCFS, and the temperature decrease with increase of $\rho$. Then, the slowing down time in the core is shorter than that in the center region and near the LCFS. The fast ions more easily slow down in the core region comparing the center with near the LCFS, which leads to the larger heating power of the 'MORH' code in the core than those of 'FP' and 'Monte-Carlo'. In the ctr-NBI case, the heating power profiles as a function of $\rho$ are still relatively peaked though they are much broader than the birth profiles due to the finite orbit effect. The heating power of 'MORH' in the center is smaller than the

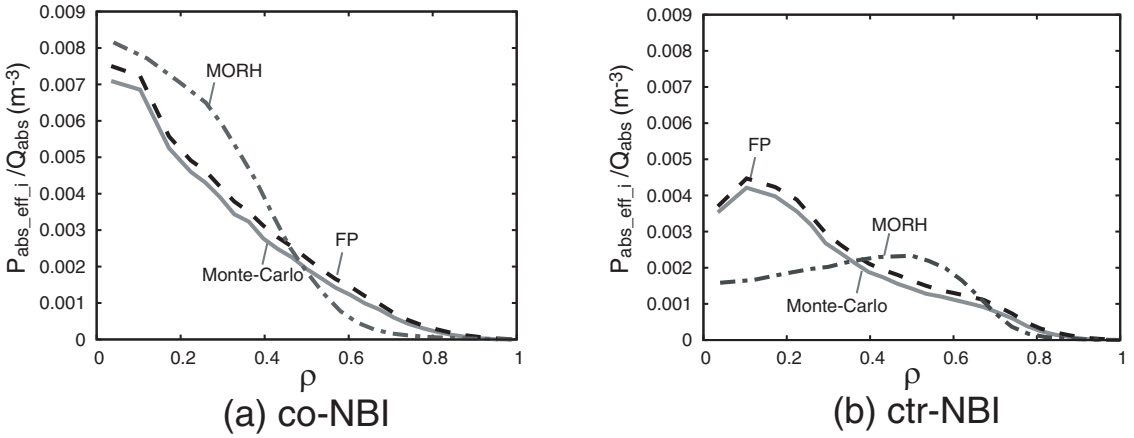


**Figure A2.** Ion heating power profiles as a function of $\rho$ for (a) the co-NBI case and (b) ctr-NBI case. Solid and dashed lines correspond to results calculated by the Monte-Carlo collision calculation and the steady state FP solution with slowing down at the birth point, respectively. The dotted dashed line corresponds to results calculated by the Monte-Carlo calculation with orbit following during slowing down, which is corresponding to the MORH's standard results.

others, and that of 'MORH' in the core is larger. The difference between the co-NBI and the ctr-NBI cases is due to the difference of the deviation between the guiding center orbits and the flux surfaces as shown in Figs. 11 (a) and (b), that is, the center of the orbits in the co-NBI case is in the inner minor radially location than that in the ctr-NBI case.

Figure A2 shows the heating power profile to the ions. Compared with Fig. A1, the heating power to the ions is tenth of that to the electrons. Comparing the shape of the heating power profile of the FP for the ions (Fig. A2) and the electrons (Fig. A1), that for ions is shrunk. The back ground ion is mainly heated by the fast ions whose energies become less than the critical energy ( $E_{\rm critical} = 15\ T_{\rm e}$ in this case ) due to the slowing down. The critical energy is reduced in proportion to the electron temperature. Thus, the heating power to the ions becomes smaller near the LCFS. In Fig. A2 as well as Fig. A1, the heating power of the 'FP' is almost same with that of the 'Monte-Carlo', but the former is a little larger than the latter, which comes from the accuracy of the steady state FP solution in the low velocity region. The tendency of the difference between 'MORH', 'FP' and 'Monte-Carlo' in the heating power to the ions, on the other hand, is almost same with that to the electrons though the heating power of 'MORH' in the core is larger than the others.

[1] A. Iiyosi et al., Nucl. Fusion **39** (1999) 1245.
[2] H. Yamada, et al., Nucl. Fusion **51** (2011) 09421.
[3] K.Y. Watanave, et al., in Proc. of ITC-17 and ISWS-16 Toki (2007) I-13.
[4] T. Hayashi et al., Contrib. Plasma Phys. **42** 2-4 (2002) 309.
[5] A. H. Boozer, Phys. Fluids **23** (1980) 904.
[6] S. Murakami, et al., Nucl. Fusion **36** (1996) 356.
[7] K. Y. Watanabe et al., Nucl. Fusion **45** (2005) 1247.
[8] HOWE, H.C., ORNL/TM-11521 (1990).

[9] K. Y. Watanabe 52nd Annual Meeting of the APS Division of Plasma Physics (2010) DI3.
[10] K. Hanatani and F. -P. Penningsfeld, Nucl. Fusion. **32** (1990) 1769.
[11] R. Seki, et al., Plasma Fusion Res. **3** (2008) 016.
[12] R. Seki *et al.,* Plasma and Fusion Res. **5** (2010) 027.
[13] T. Hayashi, Theory of Fusion Plasmas EUR 12149 EN 11 (1989).
[14] K. Harafuji, T. Hayashi and T. Sato, J. Comput. Phys. **81** (1989) 169.
[15] R. Seki *et al.,* Plasma and Fusion Res. **5** (2010) 014.
[16] H. Funaba *et al.,* Plasma and Fusion Res. **3** (2008) 022.